test results[2] are largely attributed to the inclusion of these effects in analyses. Some means, however, must be found for defining the axial and torsional flexibilities across structural joint assemblies. (These are known to be significant factors for spacecraft applications.) In addition, conversion of the empirical Alley-Ledbetter data[1] into a semiempirical formulation will enhance its usefulness for future applications.

Semiempirical Bending Flexibility Coefficients

The *empirical* Alley-Ledbetter data[1] can be converted into a semiempirical formulation involving effective properties (denoted by the subscript e) of structural joint assemblies, through the relationship

$$\theta = M(L_e/EI_e) \tag{1}$$

For mated thin-walled structural elements, it follows that for a joint assembly having a nominal diameter D,

$$\theta = (M/D^3)(8L_e/\Pi t_e E_e) \tag{2}$$

The joint assembly modulus μ_e (units of in.^{2}/lb) is defined by

$$\mu_e = 8L_e/\Pi t_e E_e \tag{3}$$

Substitution of Eq. (3) into Eq. (2) yields the semiempirical equation for the structural joint assembly bending flexibility coefficient:

$$C_B = \theta/M = \mu_e/D^3 \tag{4}$$

Values for μ_e (in.^{2}/lb) can be extrapolated from the Alley-Ledbetter data[1] (Fig. 1). Recommended values are: a) loose joint, $7(10^{-4})$; b) moderate joint, $9(10^{-5})$; c) good joint $9(10^{-6})$; and d) excellent joint, $7(10^{-7})$. These semiempirical results, as evidenced by Fig. 1, fall in the middle of the empirical Alley-Ledbetter scatter bands for the entire range of diameters.

Semiempirical Axial and Torsional Flexibility Coefficients

Semiempirical axial and torsional flexibility coefficients can be likewise derived for structural joint assemblies. The axial flexibility coefficient C_A for thin-walled elements mated by a joint assembly of nominal diameter D is described by

$$C_A = \delta/P = L_e/\Pi t_e E D \tag{5}$$

Substitution for the joint assembly modulus μ_e from Eq. (3) into Eq. (5) yields

$$C_A = \mu_e/8D \tag{6}$$

The semiempirical torsional flexibility coefficient C_T is described by

$$C_T = \phi/T = L_e/J_e G \tag{7}$$

Taking $J = 2I$ and $G = E/2(1 + \nu)$, it follows that

$$C_T = (8L_e/E\Pi t_e)(1 + \nu)/D^3 \tag{8}$$

Substitution of Eq. (3) into the Eq. (8) yields

$$C_T = [(1 + \nu)\mu_e]/D^3 \tag{9}$$

The previously cited values of μ_e as a function of joint category apply to the axial and torsional flexibility coefficient equations as well.

Conclusions

Semiempirical formulations have been established for representing the bending, axial, and torsional flexibility coefficients for structural joint assemblies. These expressions show joint flexibility to be inversely proportional to the cube of the joint assembly diameter for the bending and torsional cases, and inversely proportional to this diameter for the axial case. [The torsional case also shows a direct proportionality to Poisson's ratio in a $(1 + \nu)$ form.] The constants of proportionality are the same in each expression; different constants are required—and have been defined herein—for the four categories of structural joints identified by Alley and Ledbetter.[1] These results are necessary ingredients for, and can be applied directly in, spacecraft system and subsystem structural dynamic analyses.

References

[1] Alley, V. L. and Ledbetter, S. A., "Predictions and Measurement of Natural Vibrations of Multi-Stage Launch Vehicles," *AIAA Journal*, Vol. 1, No. 2, Feb. 1963, pp. 374–379.

[2] Kaplan, S. M. and Terkun, V., "Dynamic Analysis of the ATS-B Spacecraft," *Shock and Vibration Bulletin*, Vol. 39, No. 7, Feb. 1967, pp. 41–62.

A Solid-Propellant Rocket Motor Modulated by a Fluidic Vortex Valve

R. F. Walsh,* W. S. Lewellen,† and D. B. Stickler‡
Massachusetts Institute of Technology, Cambridge, Mass.

Nomenclature

a	=	burning rate constant ($\dot{r} = aP_s^n$)
A_c	=	control port area
A_{eff}, A_t	=	effective and geometric throat areas
M_c, M_s	=	control and supply gas molecular weights
n	=	burning rate pressure exponent ($\dot{r} = aP_s^n$)
P_s	=	combustion chamber stagnation pressure
$\dot{r}$	=	propellant linear regression rate $= aP_s^n$
r_t	=	nozzle throat radius
r_w	=	vortex valve chamber radius
T_c, T_s	=	control gas and combustion chamber stagnation temperatures
W_c, W_s	=	control and supply (propellant) mass flow divided by the maximum possible nozzle flow for the same chamber stagnation conditions
W_0	=	normalized total nozzle flow $= W_c + W_s$
β, η	=	A_{eff}/A_t and W_c/W_s, respectively

Introduction

THIS investigation was undertaken to determine the basic feasibility of modulating the burning rate of a solid propellant rocket by using a fluidic vortex valve (*VV*) controlled by a small auxiliary motor (Fig. 1). Nelson et al.[1] tested several *VV*-controlled rocket motors (*VVRM*s). They usually incorporated a bypass orifice to parallel the *VV*. The present arrangement differs from theirs in that the valve provides the only exhaust path. Keranen and Blatter[2] studied the effects of combustion gases from aluminized propellants on internal *VV* components. In their push-pull *VVRM*, they maintained a constant combustion pressure,

Presented as Paper 70-643 at the AIAA 5th Propulsion Joint Specialist Conference, San Diego, Calif., June 15–19, 1970; submitted July 6, 1970; revision received October 29, 1970. The authors acknowledge Atlantic Research Corporation for their assistance in providing propellants for the experimental portion of this work.

* NSF Graduate Fellow, Department of Aeronautics and Astronautics; now Member of the Technical Staff at Rocketdyne, Calif., Member AIAA.

† Associate Professor, Department of Aeronautics and Astronautics. Member AIAA.

‡ Assistant Professor, Department of Aeronautics and Astronautics. Member AIAA.

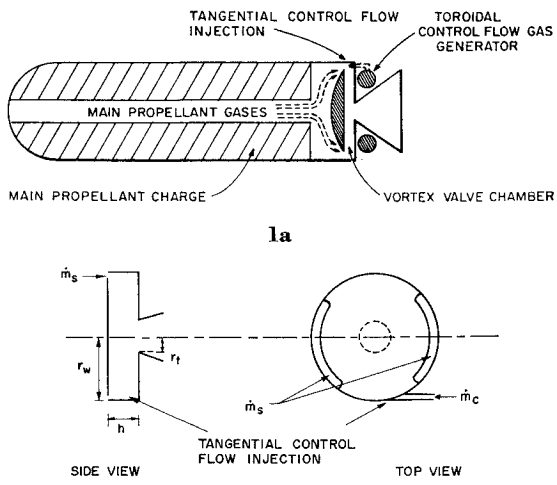

Fig. 1 Conceptual diagram of a *VV*-controlled, solid-propellant rocket motor.

while in the present experiment the equilibrium, operating combustion pressure was a prime variable.

Theoretical Model

For application to a *VVRM*, the *VV* consists of a pancake-shaped chamber (chamber radius ≫ chamber height) with radial supply flow ports and tangential control flow ports. Both control and supply flows pass through a single, centrally-located exhaust nozzle. The swirl introduced by the tangential control flow establishes a radial pressure gradient reducing the pressure at the nozzle outlet, thus reducing the outlet flow capacity. The tangential flow effectively decreases the nozzle throat area.

In Refs. 3 and 4, theoretical criteria for *VV* design have been developed. The present analysis uses the scaling law derived by Lewellen, Burns and Strickland.[4] Assuming that 1) there is no dissipation within the valve, 2) the exit stagnation pressure is approximately equal to the supply stagnation pressure, 3) the control flow injection Mach number is low enough so that control gas density changes are small, and finally 4) operation is outside the region where end-wall boundary-layer flow occurs, Lewellen et al. have shown that W_0 is a function of $W_c(r_w A_t T_c M_s / r_t A_c T_s M_c)^{1/2}$, where W_c and W_0 are mass flows normalized with respect to the maximum choked nozzle supply flow under zero swirl conditions. Using the experimental data reported by Bauer,[3] the W_0 vs W_c relation can be approximated by

$$W_c(r_w A_t T_c M_s / r_t A_c T_s M_c)^{1/2} \approx 0.191 \ln(1 - W_0) + 1.07 \quad (1)$$

Equation (1) is valid only for $W_0 \gtrsim 0.5$; in this range, since inviscid valve performance is relatively insensitive to γ,[5] Eq. (1) holds for $1.1 \leq \gamma \leq 1.4$.

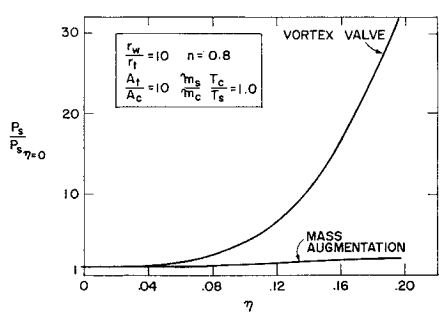

Fig. 2 Theoretical predictions of chamber pressure for a solid-propellant rocket as a function of control flow.

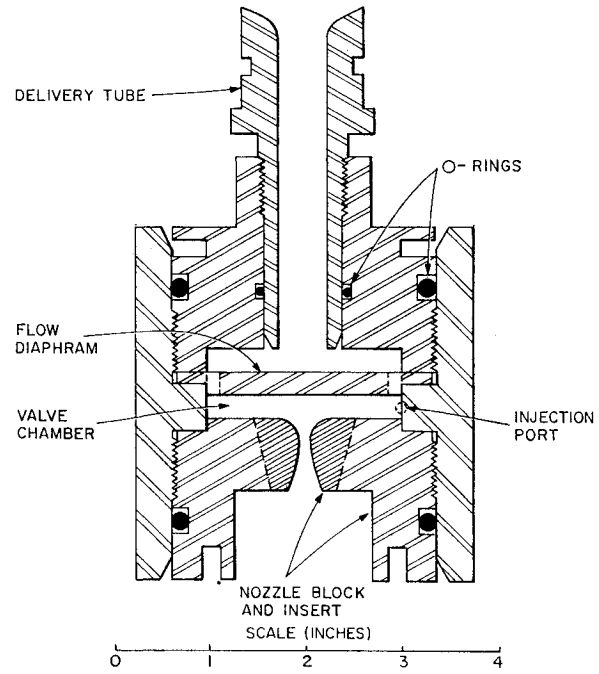

Fig. 3 Experimental valve assembly schematic.

The parameter W_s is interpreted as the effective throat area reduction, i.e., $\beta = W_s$. Since $W_0 = W_s + W_c$, and defining $\eta = W_c/W_s$, we find that $\beta = W_0/(1 + \eta)$. Assuming a propellant with $\dot{r} = aP_s^n$ and a one-dimensional isentropic nozzle mass flow, the increase in chamber pressure for the *VVRM* is

$$P_s/P_{s_{\eta=0}} = (1 + \eta/W_0)^{1/1-n} \quad (2)$$

W_0 can be eliminated from Eq. (2) (thus yielding $P_s/P_{s_{\eta=0}}$ as a function of η only) by solving Eq. (1) simultaneously with the definition of $\eta = W_0/(W_0 - W_c)$.

It is noted that valve operation yields the same increase (the $1 + \eta$ term) as straight mass augmentation (dual chamber) but has an *additional* increase of $1/W_0$. This second effect gives *VV* control a wider range of operation for the same amount of control flow expended. Vortex valving offers a greater margin of safety than a physical reduction in A_t, since perturbations in P_s can overcome the fluidic resistance, whereas a smaller A_t offers no such accommodation. This is especially important as $n \to 1$.

The performances of mass augmentation and *VV* control are compared in Fig. 2 using the following typical values: $n = 0.8$; $M_s T_c / M_c T_s = 1$; $r_w/r_t = 10$; and $A_w/A_t = 10$.

Experimental Program

An existing small solid-propellant test motor was used. Lack of internal space in the motor combustion chamber required that the vortex valve be hung externally from the motor, and the combustion gases be delivered to the valve via a short tube. A schematic of the valve assembly appears in Fig. 3. A single-port, tangential-injection control flow

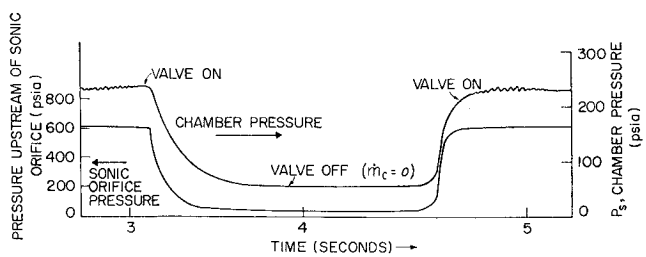

Fig. 4 Typical vortex valving test which demonstrates the response of chamber pressure to vortex valve cycling.

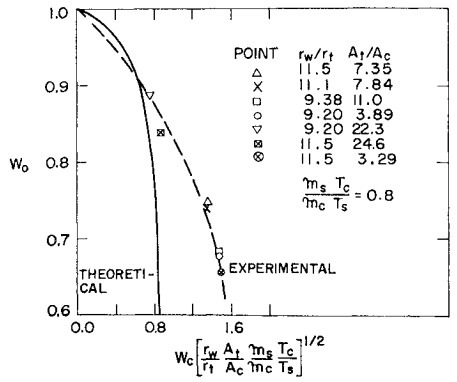

Fig. 5 Comparison of the experimental vortex valve data with theoretical predictions.

system was used. Helium at room temperature was chosen for the control gas because its ratio of T/M closely approximates T_s/M_s. The control mass flow was measured by means of an upstream sonic orifice.

The end-burning propellant[6] was a 15% aluminum, 70% ammonium perchlorate composition with carboxyl-terminated polybutadiene binder, with $n \approx 0.42$, $\dot{r} \approx 0.21$ in./sec at 300 psia, $T_s \approx 5000°$R, and $M_s \approx 30$. Graphite nozzle inserts and a pyrolytic graphite VV supply flow diaphragm were required to withstand the erosive effects of the aluminized propellant. The flow diaphragm held up remarkably well and showed less than $\frac{1}{8}$ in. stagnation-point erosion after more than 100 sec of operation. The combustion products contained almost 30% liquid Al_2O_3, much of which condensed on the internal surfaces of the motor and valve. With the valve attached to the motor, it was found that the deposited material represented 15% of the total propellant mass. This mass sink effect proved to be the greatest source of experimental uncertainty.

The control flow was cycled on and off during each run producing similar step responses in P_s (Fig. 4). The test results (normalized in terms of W_0, W_c and the scaling factor) in Fig. 5 show that performance fell short of theoretical as control flow was increased. This was not unexpected as performance may be degraded by boundary-layer effects, control flow mixing and ducting losses, heat transfer, mass sink effect, and swirl destruction causes by material deposited within the valve chamber.

Figure 6 contains the experimental data of pressure ratio vs η, and compares it with the performance that could be expected from straight mass augmentation. The error bars represent the uncertainty in total mass flow due to the mass sink effect.[6] In spite of the low burning rate exponent, the valve produced an effect over 230% greater than would be predicted for straight mass augmentation. A maximum experimental pressure ratio of 5.45 was obtained.

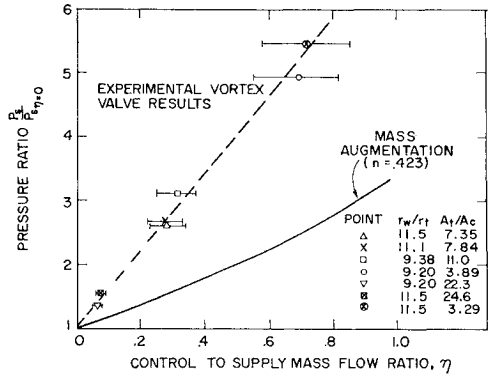

Fig. 6 Solid-propellant chamber pressure as a function of secondary flow.

Concluding Remarks

It is shown in Fig. 6 that the VV yields far better performance than mass augmentation giving the $VVRM$ greater flexibility for the same expenditure of control flow. This superiority would be even more impressive with a more efficient valve and a higher burning rate exponent (see Fig. 2). Increased stability and continuous throttling are inherent advantages of the vortex valve.

The successful performance of the pyrolytic graphite flow diaphragm is a positive indication that plates of high-temperature materials can be mounted directly in the main propellant exhaust stream. Lightweight composites (e.g., graphite, oxides, ablatives) are necessary to ensure structural integrity and minimize the condensation of exhaust products on surfaces that otherwise would have to be cooled.

Concepts such as staged series vortex valves and bidirectional control flow injection may yield further increases in system flexibility and performance.

References

[1] Nelson, C., Roberts, R., and Fish, V., "The Vortex Valve Controlled Rocket Motor," AIAA Paper 68-538, Atlantic City, N.J., 1968.

[2] Blatter, A. and Keranen, T. W., "A Vortex Valve for Flow Modulation of 5500°F Gas," *Journal of Spacecraft and Rockets*, Vol. 7, No. 2, Feb. 1970, pp. 169–174.

[3] Bauer, A. B., "Vortex Valve Operation in a Vacuum Environment," ASME Paper 68-FE-47, Philadelphia, Pa., May 1968.

[4] Lewellen, W. S., Burns, W. J., and Strickland, H. J., "Transonic Swirling Flow," *AIAA Journal*, Vol. 7, No. 7, July 1969, pp. 1290–1297.

[5] Glick, R. L. and Kilgore, M. S., "Effect of Specific Heat Ratio on Mass Flow for Swirling Nozzle Flow," *Journal of Spacecraft and Rockets*, Vol. 4, No. 8, Aug., 1967, p. 1098.

[6] Walsh, R. F., "Investigation of a Solid Propellant Rocket Motor Modulated by a Fluidic Vortex Valve," S.M. thesis, Sept. 1969, M.I.T., Cambridge, Mass.

Iterative Solution of a Radiation Dominated Heat Balance

CHARLES W. BOLZ JR.*
Rocket Research Corporation, Redmond, Wash.

Nomenclature

T_i = temperature of node i
R_{ij} = thermal resistance between nodes i and j
σ = Stefan-Boltzmann constant
$\bar{A}\bar{F}_{ij}$ = radiation interchange factor between nodes i and j
q_i = heat generation at node i
β = over-relaxation factor

Introduction

MODERN spacecraft thermal design makes extensive use of concepts such as heat shielding and multilayer insulation (superinsulation) which exploit the fourth-power temperature dependence of radiation heat transfer. However, the analytical model representing the thermal design is normally solved by numerical techniques developed for linear equations.[1] Certain of these techniques are iterative and may be extended to handle radiation heat transfer by use of a temperature-dependent radiation coefficient (radiation resistance) which is recomputed at each iteration.[2,3] This

Received October 9, 1970.
* Associate Analysis Engineer. Member AIAA.